Check for updates

ADVANCED HEALTHCARE MATERIALS
www.advhealthmat.de

Tumor-Targeted Exosome-Based Heavy Atom-Free Nanosensitizers With Long-Lived Excited States for Safe and Effective Sono-Photodynamic Therapy of Solid Tumors

Van-Nghia Nguyen, Thuy Giang Nguyen Cao, Hyunsun Jeong, Quan Truong Hoang, Binh T. T. Pham, Jieun Bang, Chang Woo Koh, Ji Hee Kang, Jeong Hyun Lee, Xiaofeng Wu, Won Jong Rhee, Young Tag Ko, K. M. K. Swamy, Sungnam Park, JaeHong Park, Min Suk Shim,* and Juyoung Yoon**

Theranostic nanosensitizers with combined near-infrared (NIR) fluorescence imaging and sono-photodynamic effects have great potential for use in the personalized treatment of deep-seated tumors. However, developing effective nanosensitizers for NIR fluorescence image-guided sono-photodynamic therapy remains a considerable challenge, including the low generation efficacy of reactive oxygen species (ROS), poor photostability, and the absence of cancer specificity. Herein, a novel heavy atom-free nanosensitizer is developed, which exhibits intense NIR fluorescence, high ROS generation efficiency, and improved aqueous stability. By conjugating a bulky and electron-rich group, 4-(1,2,2-triphenylvinyl)-1,1′-biphenyl (TPE), to the IR820 backbone, the resulting IR820 bearing TPE (IR820-TPE) effectively generates ROS via type I and II photochemical mechanisms under 808 nm laser irradiation. Moreover, TPE conjugation considerably increases the sono-photodynamic performance of IR820. To improve the intracellular delivery and tumor-targeting ability of IR820-TPE, biotin-conjugated exosome (B-Exo) is used as a natural nanocarrier. In vitro studies demonstrate the outstanding therapeutic performance of IR820-TPE-loaded B-Exo (IR820-TPE@B-Exo) in synergistic sono-photodynamic cancer therapy. In vivo studies reveal that IR820-TPE@B-Exo shows enhanced tumor accumulation, strong fluorescence signals, and effective sono-photodynamic therapeutic activity with high biosafety. This work demonstrates that IR820-TPE@B-Exo is a promising sono-phototheranostic agent for safe and targeted cancer therapy and NIR fluorescence imaging.

1. Introduction

The longstanding challenges in terms of efficacy and adverse side effects of traditional anticancer radiotherapy and chemotherapy have prompted a growing interest in the investigation and development of next-generation, high-performance cancer treatments.[1] Recently, photodynamic therapy (PDT) has attracted increasing attention and exhibits great potential as a noninvasive and localized cancer treatment modality.[2] However, PDT still suffers from a low tissue penetration depth of light which is not sufficient to achieve optimal therapeutic outcomes.[2g,3] Sonodynamic therapy (SDT), a novel noninvasive therapeutic modality using sonosensitizers combined with ultrasound (US) irradiation, has great clinical translation potential in the treatment of deep-seated solid tumors owing to the high tissue penetration depth of US.[4] Recently, sono-photodynamic therapy (SPDT), combining PDT and SDT, has become a promising approach in cancer treatment due to its synergistic anticancer activity.[5] Additionally, this combination approach can considerably decrease the intensity of US/laser required, the time of irradiation, and the dose of sensitizers, thus minimizing the adverse side effects

V.-N. Nguyen, H. Jeong, J. Bang, X. Wu, K. M. K. Swamy, J. Park, J. Yoon
Department of Chemistry and Nanoscience
Ewha Womans University
Seoul 03760, Republic of Korea
E-mail: jaehong@ewha.ac.kr; jyoon@ewha.ac.kr

V.-N. Nguyen
Department of Chemistry
School of Chemistry and Life Sciences
Hanoi University of Science and Technology
Ha Noi 100000, Vietnam

The ORCID identification number(s) for the author(s) of this article can be found under https://doi.org/10.1002/adhm.202500927

© 2025 The Author(s). Advanced Healthcare Materials published by Wiley-VCH GmbH. This is an open access article under the terms of the Creative Commons Attribution-NonCommercial License, which permits use, distribution and reproduction in any medium, provided the original work is properly cited and is not used for commercial purposes.

DOI: 10.1002/adhm.202500927

of PDT and SDT, which holds promise for personalized cancer treatment.[6]

Recently, fluorescent heptamethine cyanines have attracted widespread attention as a promising class of photosensitizers (PSs) for imaging-guided PDT due to their unique structures, favorable photophysical properties, outstanding biocompatibility, minimal background fluorescence interference, deep tissue penetration, low toxicity, and facile synthesis.[2d,7] Furthermore, heptamethine cyanine dyes also exhibit sonodynamic effects upon exposure to US irradiation.[8] Therefore, heptamethine cyanines are considered as a kind of ideal theranostic platform for imaging-guided sono-photodynamic cancer therapy. Despite significant advancements in heptamethine cyanine-based photosensitizers, their clinical translation remains hampered by limitations in ROS generation efficiency under light/US irradiation.[9] These limitations include aggregation-induced quenching, poor biocompatibility, rapid metabolism, excretion, and limited specificity toward cancer cells.[9] Therefore, along with innovative molecular design approaches to develop efficient sensitizers, exploring appropriate delivery systems that can deliver sensitizers to specific sites in a controlled manner is urgently needed to achieve improved safety, efficacy, and tumor-targeting capability.

Among the range of delivery systems developed, exosomes, nanoscale lipid-bilayer vesicles secreted by many types of cells (30–150 nm), have recently emerged as a promising nanodelivery system due to their unique advantages over conventional synthetic nanocarriers.[10] Exosomes exhibit exceptional biocompatibility, extended in vivo blood circulation, negligible toxicity, reduced immunogenicity, tumor-targeting ability, and modifiable surface structures.[10c,d] Moreover, exosomes can transport various hydrophobic and hydrophilic drugs, including chemical medicines, proteins, lipids, and nucleic acids because they are surrounded by a lipid bilayer.[10d]

Herein, we developed a novel heavy atom-free sono-PS with enhanced photochemical properties, ROS generation efficiency, and in vivo stability by conjugating a bulky electron-rich 4-(1,2,2-triphenylvinyl)-1,1′-biphenyl (TPE) group to IR820, a new indocyanine green (ICG) analog (**Figure 1**A). In addition, biotin was conjugated to exosomes to enhance their tumor-targeting capability.[11] The TPE-conjugated IR820 (IR820-TPE) was loaded into biotin-conjugated exosomes (B-Exo) for safe and tumor-targeted SPDT combined with NIR fluorescence imaging (Figure 1B). Consequently, the following advantages are offered: 1) the incorporation of the TPE group at the *meso*-position of IR820 can simultaneously enhance intersystem crossing and extend the triplet excited-state lifetime, thereby increasing ROS generation; 2) the improved ROS generation capability under light/US irradiation as compared to IR820 enables the effective treatment of deep-seated or large solid tumors; 3) the strong fluorescence intensity of the IR820-TPE is further beneficial for fluorescence imaging-guided SPDT; and 4) exosomes modified with an active cancer-targeting ligand, biotin, further improve tumor-targeted delivery. As a result, IR820-TPE-loaded, biotin-conjugated exosomes (IR820-TPE@B-Exo) can efficiently destroy tumors under dual NIR light and US irradiation via excessive generation of ROS from IR820-TPE (Figure 1B). The physicochemical characteristics of various exosomes encapsulating IR820-TPE were evaluated, and their sono-photodynamic effects were analyzed in vitro and in vivo. The resulting IR820-TPE@B-Exo can overcome the challenges of common organic PSs, and, herein, we provide ways for developing future nanosensitizers to reach clinical acceptance.

2. Results and Discussion

2.1. Molecular Design, Synthesis, Characterization, and Photophysical Properties of IR820-TPE

Heavy atom-free sensitizers offer several advantages, including lower dark toxicity, lower preparation cost, higher photostability, and longer triplet-state lifetime, compared to their counterparts containing heavy atoms.[2d] Herein, we chose IR820 as a heptamethine cyanine backbone to develop an efficient heavy atom-free sensitizer because of its superior photo-physicochemical properties compared to ICG, an FDA-approved NIR fluorescent dye used in clinical medicine. In addition, the availability of chlorine-reactive sites of IR820 enhances its functionalization.[12] The incorporation of a bulky electron-rich TPE group at the meso-position of an IR820 skeleton aimed to increase its triplet-state lifetime and photo/chemical stability, while retaining its desirable optical properties.[13] This design strategy can yield heavy atom-free IR820-TPE, a sensitizer capable of efficient ROS generation under both NIR light and US irradiation.[13]

IR820-TPE was prepared from the parent IR820 compound via one-pot synthesis using the Suzuki–Miyaura coupling reaction (Figure S1, Supporting Information). The resulting molecule was thoroughly characterized by ^{1}H nuclear magnetic resonance (NMR) spectroscopy, ^{13}C NMR spectroscopy, and mass spectrometry; the details are given in the Supporting Information (Figures S2 and S3, Supporting Information). We then evaluated the photophysical properties of IR820-TPE in dimethyl sulfoxide (DMSO). As shown in **Figure 2**A, IR820-TPE exhibited an intense ultraviolet-visible (UV-Vis) absorption band at ≈812 nm with a molar extinction coefficient nearly identical to that of IR820 (≈2 × 10^{5} M^{-1} cm^{-1}), indicating an excellent light-harvesting ability. Conversely, IR820-TPE displayed a stronger fluorescence intensity than IR820 (Figure 2B). The introduction of a TPE moiety

T. G. Nguyen Cao, Q. Truong Hoang, B. T. T. Pham, J. H. Lee, W. J. Rhee, M. S. Shim
Division of Bioengineering
Incheon National University
Incheon 22012, Republic of Korea
E-mail: msshim@inu.ac.kr
C. W. Koh, S. Park
Department of Chemistry
Korea University
Seoul 02841, Republic of Korea
J. H. Kang, Y. T. Ko
College of Pharmacy
Gachon University
Incheon 21936, Republic of Korea
W. J. Rhee
Research Center for Bio Materials & Process Development
Incheon National University
Incheon 22012, Republic of Korea
J. Yoon
Graduate Program in Innovative Biomaterials Convergence
Ewha Womans University
Seoul 03760, Republic of Korea

© 2025 The Author(s). Advanced Healthcare Materials published by Wiley-VCH GmbH

21922659, 2025, 18, Downloaded from https://advanced.onlinelibrary.wiley.com/doi/10.1002/adhm.202500927 by Ewha Womans University Library, Wiley Online Library on [07/12/2025]. See the Terms and Conditions (https://onlinelibrary.wiley.com/terms-and-conditions) on Wiley Online Library for rules of use; OA articles are governed by the applicable Creative Commons License

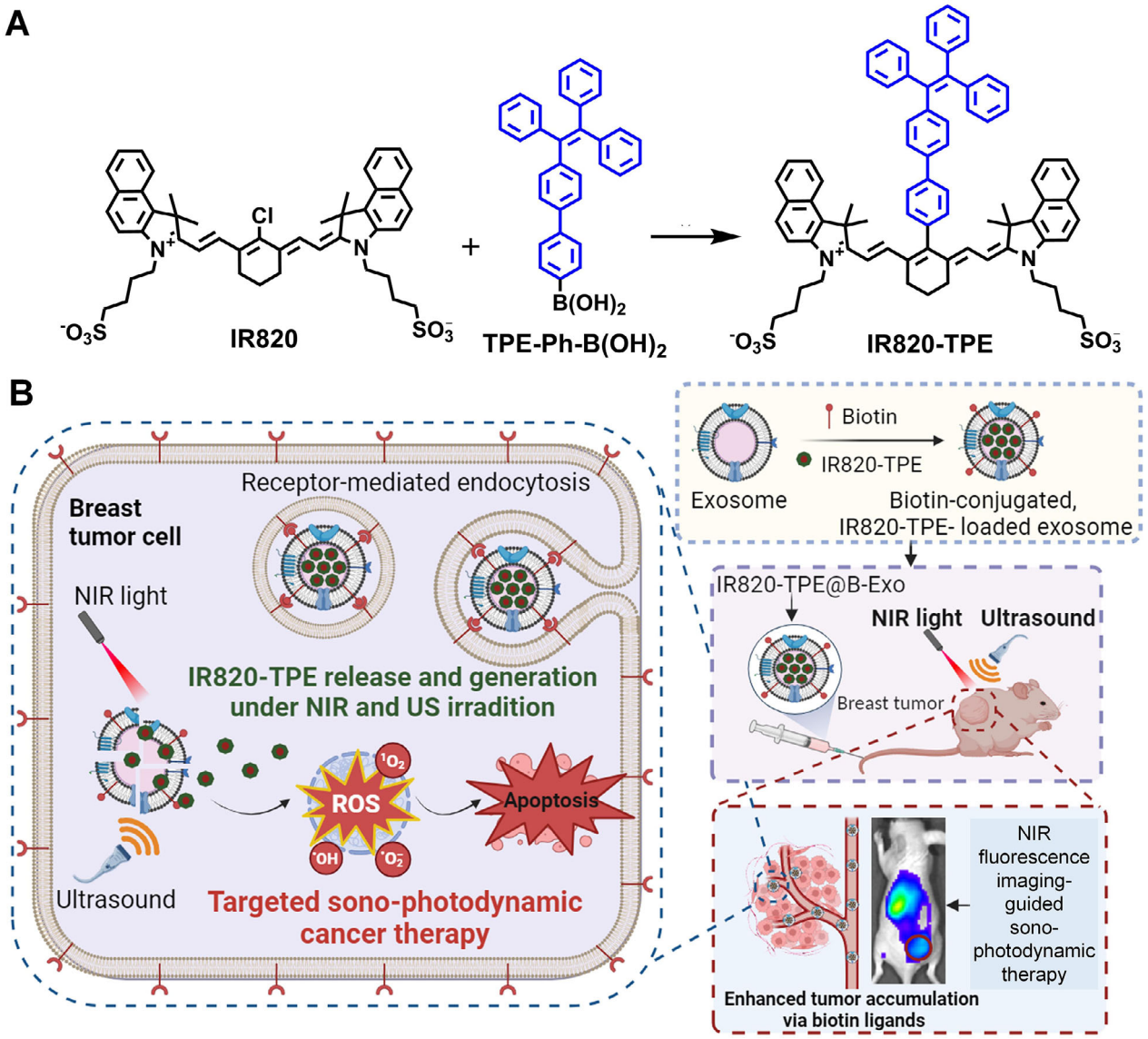


Figure 1. A) Chemical structures and synthesis route of IR820-TPE. B) Schematic illustration for the sono-photodynamic effects of IR820-TPE@B-Exo for breast tumor-targeted therapy.

into IR820 caused slight blueshifts of 20 and 8 nm in the maximum absorption and maximum emission peaks, respectively, compared to those of IR820. This result can be rationalized by the fact that the electron-donating effect of the TPE group would increase the energy level of the lowest unoccupied molecular orbital while having a lower effect on the level of the highest occupied molecular orbital. This, in turn, could lead to an increase in the band gap of IR820-TPE (blue shift),[13a,14] as shown in the density function theory (DFT) results (Figure S4, Supporting Information).

2.2. ROS Generation by IR820-TPE under NIR Light Irradiation

Inspired by the characteristic NIR light-absorbing properties of IR820-TPE, we assessed the potential of using IR820-TPE as an NIR light-triggered PDT agent. Before this evaluation, the aggregation behavior of IR820-TPE in an aqueous solution was assessed, as the aggregation state of a PS can affect its phototherapeutic efficacy. Upon dissolution in phosphate-buffered saline (PBS), both IR820 and IR820-TPE underwent self-assembly and thus formed nanoaggregates via π–π stacking interactions. Although IR820 formed severe nanoaggregates due to the strong π–π stacking interaction, nanostructures of IR820-TPE were quite stable, as illustrated in Figure S5A (Supporting Information). This observation can be attributed to the highly twisted structure of IR820-TPE. The steric bulkiness of the TPE group may prevent excessive aggregation by inhibiting strong intermolecular π–π stacking in the IR820-TPE self-assembled nanostructures compared to IR820.

To demonstrate the improved photostability of IR820 through its conjugation with TPE, we monitored the fluorescence intensities of IR820 and IR820-TPE during their incubation

© 2025 The Author(s). Advanced Healthcare Materials published by Wiley-VCH GmbH

21922659, 2025, 18, Downloaded from https://advanced.onlinelibrary.wiley.com/doi/10.1002/adhm.202500927 by Ewha Womans University Library, Wiley Online Library on [07/12/2025]. See the Terms and Conditions (https://onlinelibrary.wiley.com/terms-and-conditions) on Wiley Online Library for rules of use; OA articles are governed by the applicable Creative Commons License

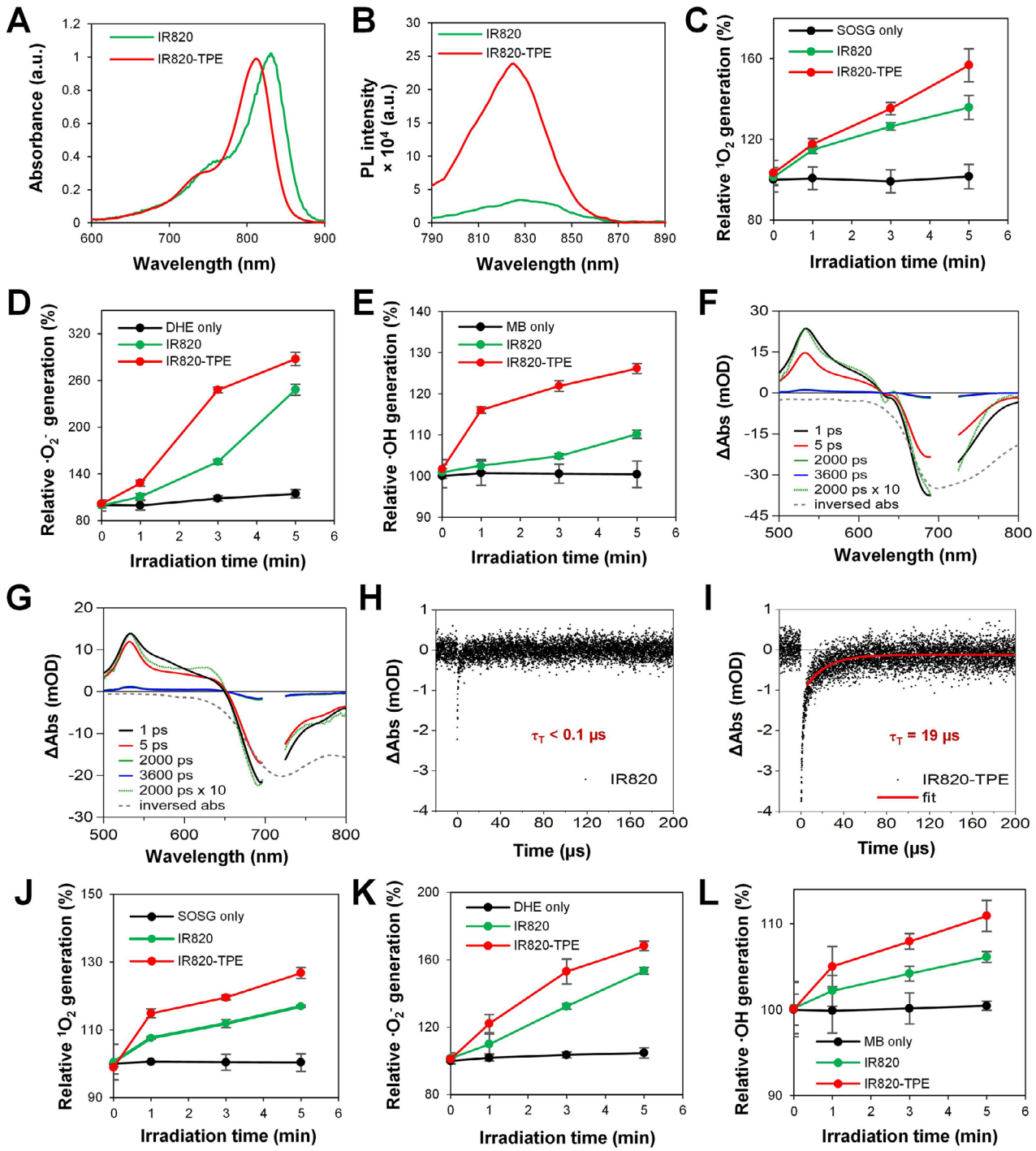


Figure 2. A) UV–vis absorption (left) and B) photoluminescence (right) spectra of IR820 and IR820-TPE (5×10^{-3} M in DMSO, $\lambda_{ex} = 780$ nm). Relative generation of C) singlet oxygen, D) superoxide anions, and E) hydroxyl radicals from IR820 and IR820-TPE in water under NIR light irradiation. Representative fs-TA spectra of F) IR820 and G) IR820-TPE in deaerated PBS solution ($\lambda_{ex} = 710$ nm, 0.26 μJ pulse^{-1}). The transient signal decay profile of H) IR820 and I) IR820-TPE from ns-TAS in deaerated PBS solution. Relative generation of J) singlet oxygen, K) superoxide anions, and L) hydroxyl radicals from IR820 and IR820-TPE in water before and after US irradiation. Data are presented as mean ± standard deviation (SD) ($n = 3$).

© 2025 The Author(s). Advanced Healthcare Materials published by Wiley-VCH GmbH

21922659, 2025, 18, Downloaded from https://advanced.onlinelibrary.wiley.com/doi/10.1002/adhm.202500927 by Ewha Womans University Library, Wiley Online Library on [07/12/2025]. See the Terms and Conditions (https://onlinelibrary.wiley.com/terms-and-conditions) on Wiley Online Library for rules of use; OA articles are governed by the applicable Creative Commons License

in PBS while exposed to NIR light. As shown in Figure S5B (Supporting Information), IR820-TPE maintained its initial fluorescent intensity more effectively than IR820, indicating the enhanced photostability of IR820-TPE than IR820. Subsequently, the ROS generation capability of IR820-TPE upon NIR irradiation was examined to evaluate its photodynamic properties. Fluorescent indicators, 2′,7′-dichlorodihydrofluorescein diacetate (DCFH-DA), singlet-oxygen sensor green (SOSG), dihydroethidium (DHE), and methylene blue (MB), were used to detect different types of ROS, including total ROS, singlet oxygen ($^1O_2$), superoxide anion ($O_2^{\bullet-}$), and hydroxyl radical ($^\bullet$OH), respectively.[15] As shown in Figure S6 (Supporting Information), upon exposure to 808 nm light, both IR820 and IR820-TPE efficiently generated ROS. Almost no ROS were generated with the DCFH-DA dye alone under 808 nm laser irradiation. IR820 and IR820-TPE also exhibited the NIR light-triggered generation of $^1O_2$ via type II photochemical reactions (Figure 2C; Figures S7 and S8, Supporting Information). Notably, the $^1O_2$ generation efficiency of IR820-TPE was much higher than that of IR820 under the same conditions (Figure 2C; Figure S7, Supporting Information). The efficient generation of $O_2^{\bullet-}$ and $^\bullet$OH by IR820 and IR820-TPE under NIR light irradiation was also demonstrated (Figure 2D, Figure S9, Supporting Information; Figure 2E, Figure S10, Supporting Information). This finding suggests that both IR820 and IR820-TPE can generate $O_2^{\bullet-}$ and $^\bullet$OH via type I photochemical reactions (Figure S8, Supporting Information). IR820-TPE demonstrated a more efficient production of $O_2^{\bullet-}$ and $^\bullet$OH compared to IR820, similar to its $^1O_2$ production.

To further validate the capability of IR820-TPE to generate ROS, the electron spin resonance (ESR) spin-trapping technique was applied with 2,2,6,6-tetramethylpiperidine ($^1O_2$-trapping agent) and 5,5-dimethyl-1-pyrroline *N*-oxide ($O_2^{\bullet-}$- and $^\bullet$OH-trapping agents).[16] IR820-TPE displayed distinct characteristic signals of $^1O_2$, $O_2^{\bullet-}$, and $^\bullet$OH upon 808 nm light irradiation, which were superior to those of IR820 (Figure S11, Supporting Information). Conversely, IR820-TPE and IR820 did not exhibit strong signals of ROS without light activation (Figure S11, Supporting Information). We hypothesize that introducing a sterically bulky TPE group into the IR820 core may lead to highly twisted molecular structures, which are essential for limiting the isomerization processes, preventing excessive aggregation by inhibiting strong intermolecular π–π stacking of IR820 dyes and decreasing self-absorption.[7b,13,17] In addition, the electron-donating effect of TPE is considerably favorable for enhancing ROS generation in IR820-TPE.[13b] Overall, these results demonstrate that IR820-TPE can be a promising PS that works via both type I and type II photoreaction mechanisms, showing high potential for efficient PDT under hypoxia.

2.3. Transient Absorption Spectroscopic Measurement

To gain insights into the formation of the triplet-state population and the consequent production of ROS, femtosecond transient absorption spectroscopy (fs-TAS) was conducted for IR820 dyes in N_2-saturated PBS solution. Figure 2F,G displays the representative transient absorption spectral evolution up to t_{delay} = ≈3600 ps of IR820 and IR820-TPE upon photoexcitation at 710 nm. Negative spectral signatures spanning from 650 to 800 nm that match the inversed steady-state absorption (gray dashed lines) originated from the depletion of a ground state (ground-state bleaching, GSB) upon photoexcitation, showing the dynamics of ground-state recovery. For both IR820 and IR820-TPE, the induced absorption (IA) band between ≈500 and ≈650 nm emerges instantaneously, which is ascribed to $S_1 \rightarrow S_n$ absorptive manifolds. Although each IA band at t_{delay} = ≈1 ps for IR820 and IR820-TPE appears virtually identical, the spectral deviation for IR820-TPE from IR820 appears prominent at t_{delay} = ≈2000 ps, with the emergence of a new additional IA band at ≈640 nm for IR820-TPE (Figure 2F,G, Figure S12, Supporting Information). This additional IA band at 640 nm for IR820-TPE persists over our instrumental limit of t_{delay} = ≈3600 ps (Figure S12B, Supporting Information) and is ascribed to the $T_1 \rightarrow T_n$ absorptive manifolds, resulting from the $S_1 \rightarrow T_n$ intersystem crossing process. This long-lived excited state for IR820-TPE in N_2-purged PBS solution was further analyzed using nanosecond transient absorption spectroscopy (ns-TAS) upon the photoexcitation at 680 nm. While almost no long-lived (<0.1 µs) transient signal at λ_{pr} = 680 nm was observed for IR820 (Figure 2H), the transient signal probed at λ_{pr} = 725 nm, which is associated with GSB for IR820-TPE, displays a decay time constant of ≈19 µs (Figure 2I). This longer lifetime of the triplet state in IR820-TPE accounts for the enhanced ROS generation of IR820-TPE compared to IR820.

2.4. Sonodynamic Effects of IR820-TPE

Inspired by the promising photodynamic performance of IR820-TPE, we investigated the ability of IR820-TPE to generate ROS under US irradiation. As shown in Figure S13 (Supporting Information), both IR820 and IR820-TPE produced ROS when exposed to US irradiation. Conversely, negligible ROS production was observed with the DCFH-DA dye alone when exposed to US irradiation. The efficient production of $^1O_2$, $O_2^{\bullet-}$, and $^\bullet$OH from IR820 and IR820-TPE under US irradiation was demonstrated using SOSG, DHE, and MB assays, respectively.[16] Notably, the US-triggered production of $^1O_2$, $O_2^{\bullet-}$, and $^\bullet$OH from IR820-TPE was more pronounced than that from IR820 (Figure 2J–L, Figures S14–S16, Supporting Information). To provide direct evidence for the enhanced ROS production capability of IR820-TPE, the generation of $^1O_2$, $O_2^{\bullet-}$, and $^\bullet$OH by IR820 under US irradiation was detected using the ESR spin-trapping technique. Under US irradiation, IR820-TPE exhibited considerably stronger ESR signals characteristic of $^1O_2$, $O_2^{\bullet-}$, and $^\bullet$OH compared to IR820 (Figure S17, Supporting Information). This demonstrates the crucial role of the TPE group in enhancing the sonodynamic performance of IR820. ESR signals were not observed for both IR820 and IR820-TPE without US treatment. These results demonstrated the exceptional photodynamic and sonodynamic effects of IR820-TPE, offering great promise for treating large or deep-seated tumors.

2.5. Preparation and Characterization of IR820-TPE-Loaded Exosomes

Herein, HEK-293T cell-derived exosomes were used because their molecular profiles were well-characterized.[18] Moreover, due to their minimal immunological response and minimal

© 2025 The Author(s). Advanced Healthcare Materials published by Wiley-VCH GmbH

21922659, 2025, 18, Downloaded from https://advanced.onlinelibrary.wiley.com/doi/10.1002/adhm.202500927 by Ewha Womans University Library, Wiley Online Library on [07/12/2025]. See the Terms and Conditions (https://onlinelibrary.wiley.com/terms-and-conditions) on Wiley Online Library for rules of use; OA articles are governed by the applicable Creative Commons License

toxicity in animal experiments, HEK-293T cells were utilized to isolate the exosomes as safe and effective nanoplatforms for delivering IR820-TPE into tumor sites. To further improve the cancer specificity of exosomes, biotin as a cancer-targeting ligand was conjugated into the exosomes. Exosomes and B-Exo were loaded with IR820 or IR820-TPE using simple incubation methods, as reported previously.[10a] The absorption spectra of IR820-TPE@Exo and IR820-TPE@B-Exo displayed a characteristic peak (796 nm) representing IR820-TPE (**Figure 3A**). The distinct peak of IR820-TPE verified that it was effectively encapsulated in exosomes. The sizes of exosome samples were ≈120 nm (Table S1, Supporting Information) and exhibited negative surface charges (Figure S18, Supporting Information). The loading efficiencies of IR820 and IR820-TPE after exosome encapsulation were 28.3% and 28.6%, respectively. The loading efficiency of IR820-TPE in IR820-TPE@B-Exo was 28.5%. The loading capacities of IR820 and IR820-TPE were determined to be 2.31×10^{-10} μg exosome^{-1} and 2.33×10^{-10} μg exosome^{-1}, respectively. The loading capacity of IR820-TPE in IR820-TPE@B-Exo was 2.38×10^{-10} μg exosome^{-1}. The amount of biotin-conjugated to the exosome surface was 5.96×10^{-11} μmol biotin/exosome. Western blotting visualized exosome markers (CD63, CD81, Hsc70, TSG101) in both blank exosomes and IR820-TPE@B-Exo, indicating no significant changes in their protein compositions during surface modification and drug loading (Figure S19, Supporting Information). The morphologies of blank exosomes and IR820-TPE@B-Exo were spheres with diameters ranging from 60 to 80 nm, as observed by transmission electron microscopy (TEM) (Figure 3B). The nanoscale diameters of the exosome samples can improve their cellular uptake, tumor accumulation, and pharmacokinetic properties.

To assess whether exosomes can protect IR820-TPE from degradation in aqueous solutions, we quantified the fluorescence intensities of IR820-TPE and IR820-TPE@Exo while they were incubated in PBS at 4 °C. As illustrated in Figure S20 (Supporting Information), IR820-TPE@Exo maintained initial fluorescence intensities of IR820-TPE at levels exceeding 85% after 14 days of incubation. In contrast, the free IR820-TPE solution exhibited a significant decrease in fluorescence after 14 days of incubation, thus confirming its poor aqueous stability. This result demonstrates the enhanced aqueous stability of IR820-TPE by encapsulation into exosomes.

2.6. Enhanced Sono-Photostability of IR820-TPE

Evaluating the degradation ratios of sono-PSs after dual NIR light-US irradiation is crucial for determining its long-term clinical viability and potential for repeated use. The degradation ratios of IR820 and IR820-TPE after NIR light and dual NIR light-US irradiation were quantified using mass spectroscopy. As depicted in Figure S21 (Supporting Information), NIR light irradiation resulted in 59.8% and 90.9% of IR820 and IR820-TPE remaining intact, respectively. Similarly, after US irradiation, 47.4% of IR820-TPE remained intact compared to 34.8% of IR820. This result demonstrates that IR820-TPE is more stable than IR820 under both NIR light and dual NIR light-US irradiation, consistent with the observed trends in fluorescence intensity changes (Figure S5B, Supporting Information). The enhanced sono-photostability of IR820-TPE suggests its high potential as an SPDT agent.

2.7. Enhanced Sono-Photostability of IR820-TPE-Loaded Exosomes

To assess the sono-photostability and sono-photodynamic potential of IR820-TPE and IR820-TPE@Exo, their fluorescence intensities under NIR light or a combination of NIR light and US irradiation were quantified in cell-free systems. As shown in Figure S22 (Supporting Information), the fluorescence intensity emitted from IR820-TPE after 2 min of NIR light irradiation decreased significantly to 38.0% of its initial value. The following US irradiation (2 min) further decreased the fluorescence intensity to 19.1% of its initial value. However, the sono-photostability of IR820-TPE in aqueous solution was markedly enhanced by the encapsulation in exosomes. NIR light irradiation for 2 min resulted in IR820-TPE@Exo retaining ≈80% of its initial fluorescence. Likewise, IR820-TPE@Exo retained ≈41.7% of its initial fluorescent intensity value even after dual NIR light (2 min) and US (2 min) irradiation. While IR820-TPE exhibited significant sono-photobleaching after dual NIR light-US irradiation, the encapsulation of IR820-TPE in the exosome remarkably improved its sono-photostability, representing one of the key achievements in this study. This result also demonstrates the high sono-photodynamic potential of IR820-TPE@Exo for ROS generation.

2.8. Enhanced Sono-Photodynamic Effects of IR820-TPE-Loaded Exosomes

To determine whether IR820- and IR820-TPE-loaded exosomes can generate ROS under NIR or US irradiation, their relative ROS production before and after NIR light or US irradiation was quantified in cell-free systems. The generation of ROS from IR820, IR820-TPE, IR820@Exo, and IR820-TPE@Exo was substantially increased with NIR light (Figure S23A, Supporting Information) or US irradiation (Figure S23B, Supporting Information). Notably, when compared to free IR820 or IR820-TPE, both IR820@Exo and IR820-TPE@Exo exhibited a higher efficacy in ROS generation. This result could be attributed to the improved aqueous stability of IR820 and IR820-TPE via encapsulation into exosomes (Figures S5B and S22, Supporting Information). In addition, ROS production in IR820-TPE@Exo-treated MCF-7 cells was amplified 6.1-fold by the combined treatment of NIR light and US compared to untreated controls (Figure S24, Supporting Information). The ROS generation efficiency of IR820-TPE under NIR light irradiation alone and with dual NIR light-US irradiation was compared. Sequential treatment with NIR light irradiation followed by US irradiation led to further ROS generation by both IR820-TPE and IR820-TPE@Exo (Figure S25, Supporting Information). These results demonstrate the potential of IR820-TPE@Exo as effective sono-PSs for SPDT.

2.9. Enhanced Cancer-Targeted Cellular Uptake of IR820-TPE@B-Exo

To investigate whether exosomes can enhance the intracellular delivery of therapeutic drugs, cellular uptake of IR820, IR820-

© 2025 The Author(s). Advanced Healthcare Materials published by Wiley-VCH GmbH

21922659, 2025, 18, Downloaded from https://advanced.onlinelibrary.wiley.com/doi/10.1002/adhm.202500927 by Ewha Womans University Library, Wiley Online Library on [07/12/2025]. See the Terms and Conditions (https://onlinelibrary.wiley.com/terms-and-conditions) on Wiley Online Library for rules of use; OA articles are governed by the applicable Creative Commons License

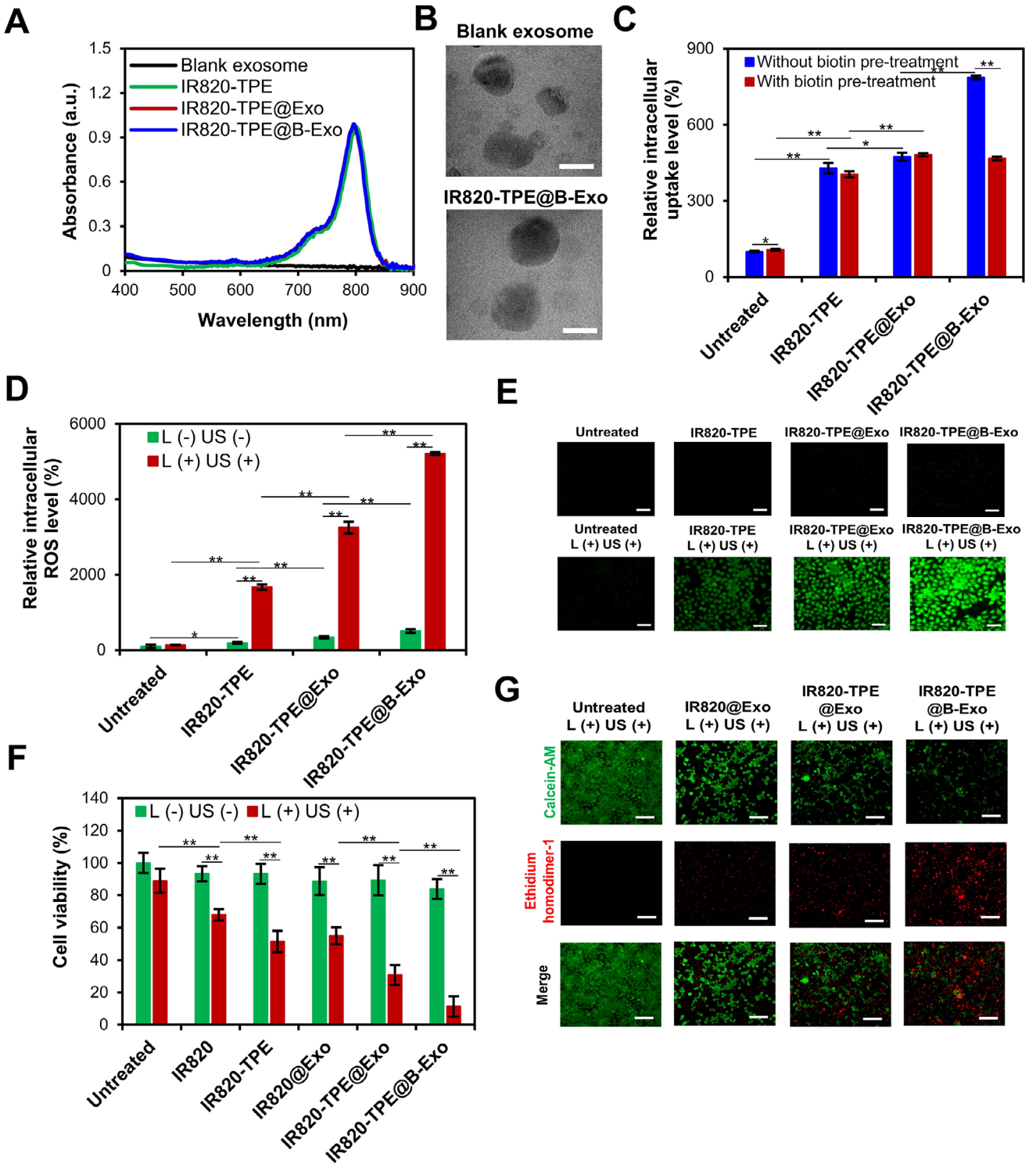


Figure 3. A) Absorption spectra of blank exosome, IR820-TPE, IR820-TPE@Exo, and IR820-TPE@B-Exo. B) TEM images of blank exosome and IR820-TPE@B-Exo. Scale bars indicate 50 nm. C) Relative cellular uptake of IR820-TPE in MCF-7 cells after incubation with IR820-TPE, IR820-TPE@Exo, and IR820-TPE@B-Exo for 4 h with and without biotin pretreatment. D) Intracellular ROS levels and E) Fluorescence images of DCF-DA-stained MCF-7 cells treated with IR820-TPE, IR820-TPE@Exo, and IR820-TPE@B-Exo before and after irradiation with NIR light or NIR light + US. Scale bar = 100 μm. F) Viabilities and G) Fluorescence images of MCF-7 cells after treatment with various samples before and after irradiation with NIR light and US. The cells were costained with calcein AM (live cells, green) and ethidium homodimer-1 (dead cells, red). Scale bar = 200 μm. Data are presented as mean ± SD ($n = 3$, $^{*}p < 0.05$, $^{**}p < 0.01$).

© 2025 The Author(s). Advanced Healthcare Materials published by Wiley-VCH GmbH

21922659, 2025, 18, Downloaded from https://advanced.onlinelibrary.wiley.com/doi/10.1002/adhm.202500927 by Ewha Womans University Library, Wiley Online Library on [07/12/2025]. See the Terms and Conditions (https://onlinelibrary.wiley.com/terms-and-conditions) on Wiley Online Library for rules of use; OA articles are governed by the applicable Creative Commons License

TPE, IR820@Exo, and IR820-TPE@Exo by MCF-7 human breast cancer cells was examined at an equivalent concentration of IR820 or IR820-TPE. IR820@Exo and IR820-TPE@Exo exhibited a considerable increase in the cellular uptake of IR820 or IR820-TPE when compared to free IR820 or IR820-TPE (Figure S26, Supporting Information). The favorable interaction of exosomes with cell membranes via receptor–ligand binding or direct fusion may lead to considerable improvement in the cellular uptake of IR820 and IR820-TPE.[19] The biotin moiety of exosomes could facilitate their cellular uptake via biotin receptor-mediated endocytosis, especially in MCF-7 cells due to their overexpression of biotin receptors.[11] As shown in Figure 3C, IR820-TPE@B-Exo was more efficiently internalized by the MCF-7 cells compared to biotin-free IR820-TPE@Exo or IR820-TPE. This result reveals the cancer-selective cellular uptake of IR820-TPE@B-Exo. In addition, a biotin competition binding experiment was conducted to demonstrate the role of biotin in the receptor-mediated endocytosis of IR820-TPE@B-Exo. Herein, MCF-7 cells were pretreated with free biotin before the treatment with IR820-TPE, IR820-TPE@Exo, and IR820-TPE@B-Exo. As shown in Figure 3C, preincubation of biotin with MCF-7 cells markedly reduced the cellular uptake of IR820-TPE@B-Exo owing to the excess of biotin-blocking biotin receptors in the cells before the treatment with IR820-TPE@B-Exo. This finding suggests a direct correlation between the promoted uptake of IR820-TPE@B-Exo by MCF-7 cells and biotin receptor–mediated endocytosis.

2.10. Efficient ROS Generation of IR820-TPE@B-Exo in MCF-7 Cells after NIR Light and US Irradiation

Intracellular ROS levels in MCF-7 cells were measured using a ROS-sensitive DCFH-DA before and after NIR light, US, or NIR light + US irradiation after various treatments. As shown in Figure S27 (Supporting Information), cells treated with IR820-TPE produced ROS more efficiently than IR820-treated cells under NIR light and US irradiation. This result was also confirmed by fluorescence imaging (Figure S28, Supporting Information). Notably, MCF-7 cells treated with IR820-TPE, IR820-TPE@Exo, and IR820-TPE@B-Exo exhibited a remarkable increase in the levels of intracellular ROS after exposure to NIR light (Figure S29, Supporting Information) or US exposure (Figure S30, Supporting Information). Irrespective of irradiation with NIR light and US, MCF-7 cells treated with IR820-TPE-loaded exosomes exhibited higher levels of intracellular ROS compared to those treated with IR820-TPE (Figures S29 and S30, Supporting Information). This finding might be because of the enhanced cellular uptake of the IR820-TPE via encapsulation into exosomes (Figure 3C). Remarkably, IR820-TPE@B-Exo also exhibited a considerable increase in the levels of ROS in MCF-7 cells compared to IR820-TPE@Exo (Figure 3D). The enhanced intracellular ROS generation by IR820-TPE@B-Exo compared to IR820-TPE@Exo might be attributed to its increased cellular uptake. The highest intracellular ROS levels were observed in the cells treated with IR820-TPE@B-Exo under irradiation with a combination of NIR light and US (Figure 3D).

Intracellular ROS levels in DCFH-DA-stained MCF-7 cells after various treatments were further verified by fluorescence imaging (Eclipse Ti-S). The strongest fluorescence signals were observed in the cells treated with IR820-TPE@B-Exo after irradiation with a combination of NIR light and US (Figure 3E). This result highlights the high potency of IR820-TPE@B-Exo for efficient SPDT in breast cancer cells.

2.11. In Vitro Cancer-Targeted SPDT Using IR820-TPE@B-Exo

Sono-photodynamic anticancer activity of various IR820-TPE and IR820-TPE@B-Exo samples against MCF-7 cells was investigated. The cytotoxicity of IR820-TPE or IR820-TPE@B-Exo in MCF-7 cells at different concentrations of IR820-TPE or IR820-TPE@B-Exo was evaluated to optimize the dose for efficient SPDT effects with minimal adverse effects. As shown in Figures S23 and S31 (Supporting Information), higher IR820-TPE or IR820-TPE@B-Exo concentrations led to higher cytotoxicity, irrespective of irradiation with light or US. Due to the potential for severe dark cytotoxicity (cytotoxicity in the absence of light) at high concentrations of IR820-TPE@B-Exo, the optimized concentration of IR820-TPE@B-Exo was determined to be 5×10^{-6} M of IR820-TPE.

The cytotoxic effects of IR820, IR820-TPE, IR820@Exo, IR820-TPE@Exo, and IR820-TPE@B-Exo in MCF-7 cells were determined before and after NIR light + US irradiation. As shown in Figure 3F, NIR + US irradiation exhibited a negligible cytotoxic effect on MCF-7 cells. More than 88.9% of MCF-7 cells remained viable after 2 min of NIR light irradiation and 2 min of US irradiation (Figure 3F). MCF-7 cells exposed to IR820@Exo exhibited lower viability than those exposed to free IR820, which is attributed to the enhanced uptake of IR820 by exosomes. Similarly, IR820-TPE@Exo showed considerable cytotoxicity compared to free IR820-TPE. Notably, MCF-7 cells treated with IR820-TPE exhibited a significant decrease in their viability compared to IR820 under dual NIR light-US irradiation (Figure 3F). The enhanced cytotoxicity by IR820-TPE compared to IR820 might be attributed to its higher sono-photodynamic effects for ROS generation (Figure S27, Supporting Information). IR820-TPE, IR820-TPE@Exo, and IR820-TPE@B-Exo groups displayed significant cytotoxicity after combined irradiations of NIR light and US (Figure 3F), demonstrating their high potential for sono-photodynamic combination cancer therapy. The treatment of MCF-7 cells with IR820-TPE@B-Exo under dual NIR light-US irradiation demonstrated the highest cytotoxicity (Figure 3F). For example, only 11.4% of cells remained viable after SPDT of IR820-TPE@B-Exo. The most efficient IR820-TPE uptake by the B-Exo could be responsible for the highest cytotoxicity (Figure 3C). These results reveal that the IR820-TPE-loaded exosomes are effective sono-PSs.

To investigate the individual contribution of NIR light and US on the SPDT activity of IR820-TPE and IR820-TPE-loaded exosomes, the viabilities of MCF-7 cells after various treatments under irradiation of NIR light, US, or dual NIR light-US were measured. As shown in Figure S33 (Supporting Information), IR820-TPE, IR820-TPE@Exo, and IR820-TPE@B-Exo reduced cell viability under NIR light or US irradiation. The cytotoxicities of the IR820-TPE, IR820-TPE@Exo, and IR820-TPE@B-Exo groups under NIR light irradiation were comparable to those observed with US irradiation (Figure S33, Supporting Information). No-

© 2025 The Author(s). Advanced Healthcare Materials published by Wiley-VCH GmbH

21922659, 2025, 18, Downloaded from https://advanced.onlinelibrary.wiley.com/doi/10.1002/adhm.202500927 by Ewha Womans University Library, Wiley Online Library on [07/12/2025]. See the Terms and Conditions (https://onlinelibrary.wiley.com/terms-and-conditions) on Wiley Online Library for rules of use; OA articles are governed by the applicable Creative Commons License

tably, the combination of NIR light and US irradiation synergistically reduced the viability of MCF-7 cells when treated with IR820-TPE, IR820-TPE@Exo, and IR820-TPE@B-Exo, demonstrating their potential of SPDT. Intracellular ROS levels of MCF-7 cells after treatment with IR820-TPE@B-Exo were evaluated under NIR light, US, or dual NIR light-US irradiation. IR820-TPE@B-Exo significantly increased the level of intracellular ROS under NIR light or US irradiation (Figure S34, Supporting Information). Notably, the combination of NIR light and US irradiation synergistically enhanced the production of intracellular ROS.

To investigate how the sequence of NIR light and ultrasound (US) irradiation affects the SPDT efficacy of IR820-TPE@Exo, we evaluated its intracellular ROS generation capability under different irradiation sequences. MCF-7 cells treated with IR820-TPE@Exo exhibited substantially higher intracellular ROS levels when exposed to NIR light followed by US irradiation, compared to the reverse sequence (US followed by NIR light irradiation) (Figure S35A, Supporting Information). This sequence-dependent ROS generation by IR820-TPE@Exo proved critical to its anticancer activity. As shown in Figure S35B (Supporting Information), exposure to US irradiation followed by NIR light reduced cell viability to 69.6%, while reversing the irradiation sequence (NIR light irradiation before US irradiation) resulted in a much higher decrease to 36.8%. The sequence of NIR light followed by US irradiation yielded a higher synergistic enhancement in the SPDT efficacy of IR820-TPE@Exo than the reverse sequence. This might be due to the preactivation of the IR820-TPE by NIR light, which increases its susceptibility to the effects of subsequent US treatment.

To examine the cancer-targeting effect of IR820-TPE@B-Exo, a cytotoxicity quantification in human breast cancer cells MCF-7 and human dermal fibroblast cells (hDFB) was carried out. As shown in Figure S36 (Supporting Information), the IR820-TPE@Exo treatment without light and US irradiation did not cause strong toxicity to both MCF-7 and hDFB cells. However, the toxicity of IR820-TPE@B-Exo against MCF-7 cells was dramatically higher than IR820-TPE@Exo regardless of NIR light and US irradiation, whereas no significant difference was observed in hDFB cells. This outcome might be explained by the cancer-specificity of IR820-TPE@B-Exo. Importantly, under NIR light and US exposure, the IR820-TPE@B-Exo treatment remarkably reduced the viability of MCF-7 cells compared to hDFB cells while no substantial difference in the treatment of IR820-TPE@Exo in MCF-7 and hDFB cells. This result demonstrated the cancer-specific SPDT of IR820-TPE@B-Exo.

SPDT activities of IR820@Exo, IR820-TPE@Exo, and IR820-TPE@B-Exo in MCF-7 cells were visualized by fluorescence imaging of the sample-treated cells after staining with calcein acetoxymethyl ester (calcein AM, green, living cells) and ethidium homodimer-1 (EthD-1, red, dead cells). Figure 3G displays the fluorescence images of costained MCF-7 cells after various treatments under NIR light + US irradiation. All the groups showed marked cell death after dual irradiations, resulting in strong red fluorescence signals. The cells exposed to IR820-TPE@B-Exo and dual irradiations exhibited the lowest viability, which was consistent with the cytotoxicity results (Figure 3F).

To investigate whether the sono-photodynamic effects of IR820-TPE@Exo induced apoptosis, we quantified the apoptotic rate of MCF-7 cells treated with various samples before and after irradiation with NIR light + US. As shown in Figure S37 (Supporting Information), when the cells were treated with IR820@Exo, IR820-TPE@Exo, and IR820-TPE@B-Exo, the population of total apoptotic cells (early apoptosis + late apoptosis) considerably increased under NIR light and US irradiation. Notably, the combination of PDT and SDT markedly increased the percentage of total apoptotic cells of the IR820-TPE@B-Exo group to 84.93%. These results indicate that SPDT by IR820-TPE-based samples triggers significant apoptosis in MCF-7 cells.

The expression of Caspase-3/7 in MCF-7 cells was analyzed to demonstrate the apoptosis of MCF-7 cells after sono-photodynamic treatment of IR820-TPE@B-Exo. As shown in Figure S38 (Supporting Information), the expression of Caspase-3/7 in MCF-7 cells treated with IR820-TPE@B-Exo under NIR light and US irradiation was significantly increased compared to that in MCF-7 cells treated with IR820-TPE@B-Exo only. This result is consistent with the apoptosis results evaluated by Annexin V-FITC/PI labeling (Figure S37, Supporting Information).

2.12. Effective Tumor Accumulation of IR820-TPE@B-Exo

It is well documented that exosomes can efficiently accumulate in tumors via EPR effects.[20] To assess in vivo tumor accumulation of various exosome samples, in vivo real-time fluorescence imaging of MCF-7-xenograft mice was conducted following intravenous (i.v.) administration of the different exosome samples. The biodistribution of free IR820, free IR820-TPE, IR820-TPE@Exo, and IR820-TPE@B-Exo in the MCF-7-xenograft mice at different time intervals (0–24 h postinjection) was visualized using an in vivo imaging system, which can detect and quantify the fluorescence signals of IR820 and IR820-TPE. All the mice groups exhibited fluorescence signals of free IR820 or IR820-TPE all over their bodies 30 min after i.v. injection (**Figure** 4A,B). However, the fluorescence of free IR820 or IR820-TPE almost disappeared from the tumor within 24 h after injection of the free IR820- or IR820-TPE-treated groups, suggesting poor tumor accumulation of free IR820 and IR820-TPE. Notably, strong fluorescence signals were observed in the tumor of mice within 24 h when they were treated with IR820-TPE@Exo and IR820-TPE@B-Exo (Figure 4C,D, Supporting Information). This finding suggests that exosomes loaded with IR820-TPE could accumulate in tumors. Moreover, the tumors in the IR820-TPE@B-Exo-treated mice exhibited higher fluorescence intensity than those in the IR820-TPE@Exo-treated mice, demonstrating more efficient tumor accumulation of IR820-TPE@B-Exo than that of IR820-TPE@Exo. The major organs and tumors of mice were harvested 24 h after the injection of the samples for ex vivo fluorescence imaging. The fluorescence signals from the major organs and tumors of mice were quantified to analyze the biodistribution of samples. As shown in Figure 4E,F, the amount of IR820-TPE localized in the tumor of the mice treated with IR820-TPE@Exo or IR820-TPE@B-Exo was considerably higher than that of the mice treated with free IR820-TPE. This result demonstrates the superior accumulation of IR820-TPE in tumors via encapsulation in exosomes. IR820-TPE@B-Exo exhib-

© 2025 The Author(s). Advanced Healthcare Materials published by Wiley-VCH GmbH

21922659, 2025, 18, Downloaded from https://advanced.onlinelibrary.wiley.com/doi/10.1002/adhm.202500927 by Ewha Womans University Library, Wiley Online Library on [07/12/2025]. See the Terms and Conditions (https://onlinelibrary.wiley.com/terms-and-conditions) on Wiley Online Library for rules of use; OA articles are governed by the applicable Creative Commons License

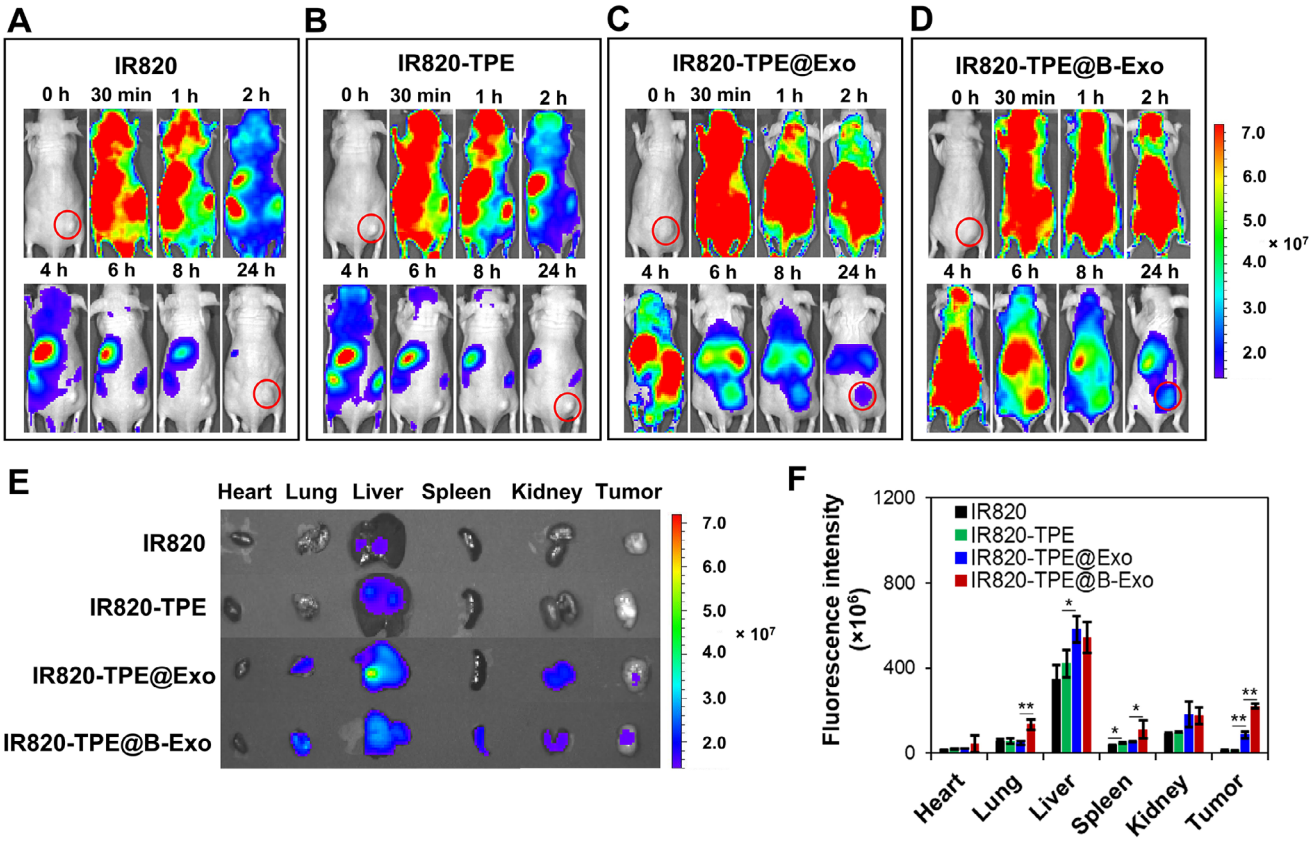


Figure 4. In vivo biodistribution images from MCF-7 tumor–xenograft mice after i.v. administration of A) IR820, B) IR820-TPE, C) IR820-TPE@Exo, and D) IR820-TPE@B-Exo. E) Ex vivo imaging of tumors and major organs. F) Quantification of IR820 and IR820-TPE from ex vivo imaging of major organs and tumors of tumor-bearing mice following i.v. administration of IR820, IR820-TPE, IR820-TPE@Exo, and IR820-TPE@B-Exo. Data are presented as mean ± SD ($n = 3$, $^*p < 0.05$, $^{**}p < 0.01$).

ited the most efficient tumor accumulation owing to the cancer-targeting ability of biotin. The quantitative results indicated that all the samples injected into mice mainly accumulated in the liver, which might be attributed to their nonspecific accumulation by the reticuloendothelial system (Figure 4F). The in vivo fluorescence imaging demonstrates that IR820-TPE@B-Exo has high potential for tumor-targeted SPDT.

To demonstrate the tumor accumulation ability of IR820-TPE@Exo and IR820-TPE@B-Exo, the fluorescence intensity ratios of tumor core areas to peritumoral tissue areas (C/P) in the IR820-TPE@Exo- and IR820-TPE@B-Exo-treated mice were measured at different time intervals after injection. As demonstrated in Figure S39 (Supporting Information), there was no significant difference in the C/P ratios of IR820-TPE@Exo- and IR820-TPE@B-Exo-treated mice at 0 h and 30 min-post injection. However, after 1 h-post injection, the C/P ratio of IR820-TPE@B-Exo-treated mice was significantly higher than that of IR820-TPE@Exo-treated mice, demonstrating that biotin conjugation to the exosome surface can enhance the tumor accumulation of IR820-TPE@B-Exo. In addition, the highest C/P ratio was observed at 4 h post-injection (Figure S39, Supporting Information). Therefore, the tumors were exposed to NIR light or US irradiation 4 h after the injection of IR820-TPE@B-Exo to maximize their SPDT efficacy in tumors.

2.13. Efficient In Vivo Tumor Inhibition by Sono-Photodynamic Effects of IR820-TPE@B-Exo

Inspired by the effective in vitro anticancer effects and tumor accumulation of IR820-TPE@B-Exo, we evaluated its in vivo tumor inhibition efficacy using MCF-7 tumor–xenograft mice models. Various samples [PBS, IR820-TPE, IR820@Exo, IR820-TPE@Exo, and IR820-TPE@B-Exo (at equivalent concentrations of IR820 and IR820-TPE)] were injected into the tail vein of the tumor-bearing mice. At 4 h after injection, the tumor area was irradiated with either NIR light (808 nm, 500 mW, 2 min), US (1 MHz, 0.5 W cm^{-2}, 2 min), or a combination of both (2 min for each). The tumor volumes were monitored for 14 days without further injections or NIR/US irradiation (Table S2, Supporting Information). The treatment of PBS + Light (L) or PBS + L + US caused negligible inhibitory effects on the growth of tumors in mice (Figure S40, Supporting Information). In contrast to the mice treated with free IR820-TPE, those treated with IR820@Exo, IR820-TPE@Exo, and IR820-TPE@B-Exo exhibited efficient inhibition of tumor growth under NIR light irradiation (**Figure 5A**). Treatment with IR820-TPE@Exo suppressed the tumor growth more efficiently than the treatment with IR820@Exo under NIR light irradiation, demonstrating the higher PDT effect of IR820-TPE than IR820. Notably, the tumor growth inhibition

© 2025 The Author(s). Advanced Healthcare Materials published by Wiley-VCH GmbH

21922659, 2025, 18, Downloaded from https://advanced.onlinelibrary.wiley.com/doi/10.1002/adhm.202500927 by Ewha Womans University Library, Wiley Online Library on [07/12/2025]. See the Terms and Conditions (https://onlinelibrary.wiley.com/terms-and-conditions) on Wiley Online Library for rules of use; OA articles are governed by the applicable Creative Commons License

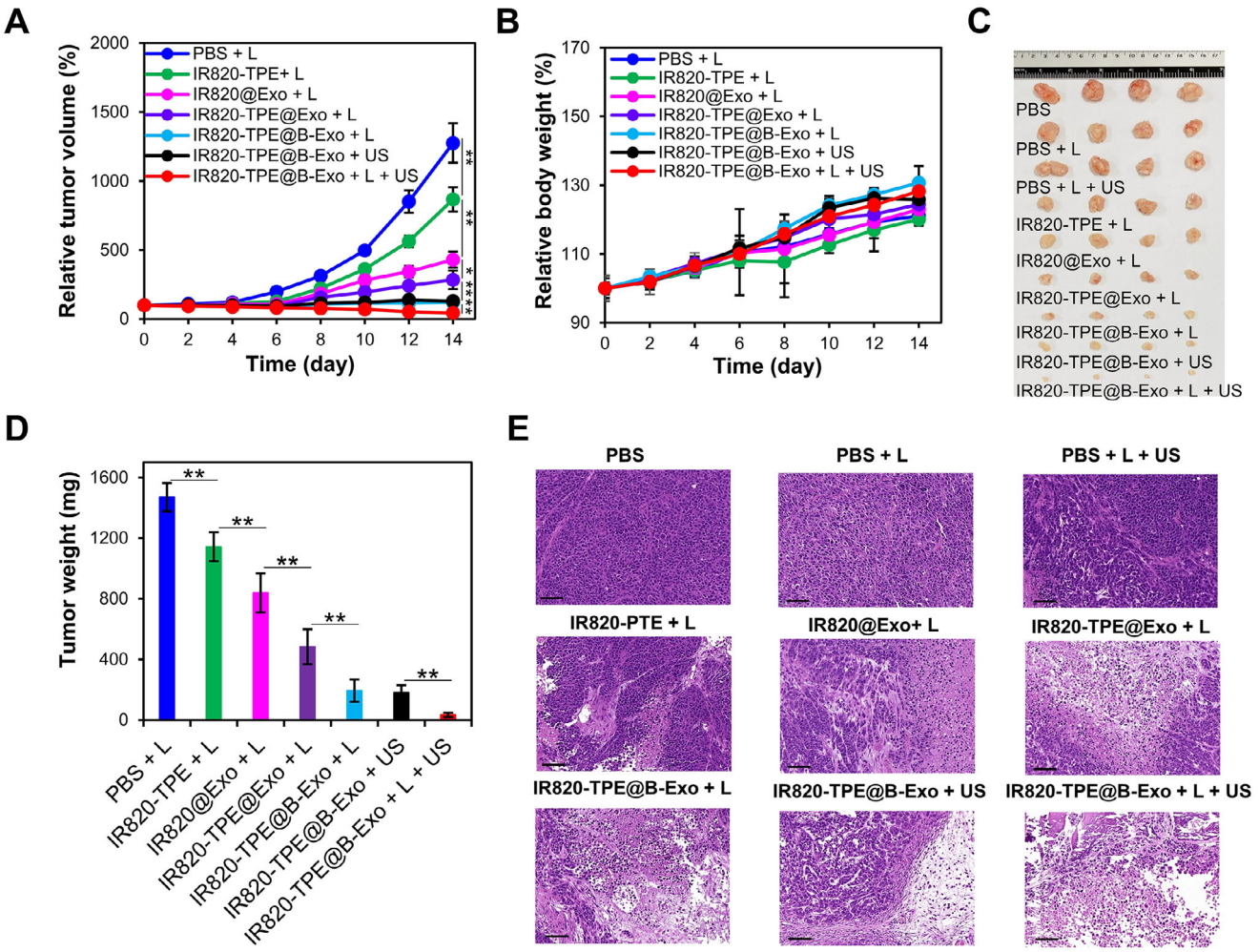


Figure 5. A) Normalized tumor growth ratio and B) Changes in the body weights of MCF-7 tumor-bearing mice ($n = 4$) for 14 days after i.v. injection of various samples under irradiation with NIR light, US or NIR light + US. The mice were irradiated with NIR light or US at 4 h post-i.v. injection of each sample. C) Representative images of tumors and D) Tumor weights of the mice on day 14 after i.v. injection of various samples under irradiation with NIR light, US, or NIR light + US. E) H&E staining of tumors of the mice on day 14 after i.v. injection of various samples under irradiation with NIR light, US, or NIR light + US. Scale bars indicate 200 μm. Data are presented as mean ± SD ($n = 4$, $^*p < 0.05$, $^{**}p < 0.01$).

of the IR820-TPE@B-Exo-treated group was more pronounced compared to other groups under NIR light irradiation. The inhibition of tumor growth by the treatment of IR820-TPE@B-Exo and US was comparable to that by the treatment of IR820-TPE@B-Exo and NIR light (Figure 5A). Treatment with IR820-TPE@B-Exo under the combination of NIR light and US irradiation [IR820-TPE@B-Exo + L + US] resulted in the most efficient suppression of tumor growth. These results demonstrate that tumor-targeting IR820-TPE@B-Exo has a high potential for safe and efficient SPDT.

The changes in the body weights of sample-treated mice reveal the acute toxicity of the injected samples. The body weights of all the tested mice groups did not considerably change during the tumor growth inhibition experiments (Figure 5B and Figure S41, Table S3, Supporting Information), indicating that the injected samples did not cause considerable systemic acute toxicity. The photographs of tumors from euthanized mice on day 14 after injection corresponded well with the results of tumor growth suppression (Figure 5C). Moreover, the average weights of the tumors in the mice treated with various samples were measured. The tumors of mice treated with IR820-TPE@B-Exo under the combination of NIR light and US irradiation had the lowest average weight (Figure 5D and Figure S42, Supporting Information), which was consistent with the results of tumor growth suppression (Figure 5A). These results indicate the high efficacy and biosafety of tumor-targeting IR820-TPE@B-Exo. Tumor tissues harvested from mice treated with various samples were analyzed using hematoxylin and eosin (H&E) staining. As shown in Figure 5E, mice treated with IR820-TPE@B-Exo under the combination of NIR light and US irradiation exhibited considerable tumor damage. H&E staining of vital organs, such as the heart, liver, lungs, spleen, and kidneys, showed that the organs from each treatment group exhibited normal cellular morphologies and negligible histological changes (Figure S43, Supporting Information). This result demonstrates the high biosafety of IR820-TPE@B-Exo.

© 2025 The Author(s). Advanced Healthcare Materials published by Wiley-VCH GmbH

21922659, 2025, 18, Downloaded from https://advanced.onlinelibrary.wiley.com/doi/10.1002/adhm.202500927 by Ewha Womans University Library, Wiley Online Library on [07/12/2025]. See the Terms and Conditions (https://onlinelibrary.wiley.com/terms-and-conditions) on Wiley Online Library for rules of use; OA articles are governed by the applicable Creative Commons License

3. Conclusion

We present a rational design strategy for developing highly efficient, heavy atom-free, NIR sensitizers based on heptamethine cyanine scaffolds for fluorescence imaging-guided sono-photodynamic cancer therapy. Our approach involves the modification of IR820 with a sterically bulky and electron-rich TPE moiety at the *meso*-position, resulting in a novel NIR sensitizer with improved fluorescence intensity and ROS generation capability under both light and US irradiation. Notably, IR820-TPE was capable of generating ROS via both type I and II mechanisms, which is beneficial for treating hypoxic tumors with low oxygen concentrations. The encapsulation of IR820-TPE in exosomes considerably enhanced its aqueous stability and cellular uptake, resulting in the increased production of ROS in response to NIR light/US irradiation. The conjugation of biotin to the exosomes further increased their cellular uptake into breast cancer cells, resulting in enhanced sono-photodynamic performance. In vivo studies revealed that IR820-TPE-loaded exosomes exhibited enhanced tumor accumulation compared to free IR820-TPE. Notably, biotin-conjugated exosomes loaded with IR820-TPE exhibited the most efficient suppression of tumor growth in tumor-bearing mice without any systemic toxicity. This study highlights the significant potential of IR820-TPE as a highly efficient sono-PS. This study also demonstrates that biotin-conjugated exosomes encapsulating IR820-TPE are safe and efficient nanosensitizers for cancer-targeted SPDT.

4. Experimental Section

Synthesis of IR820-TPE: TPE-Ph-boronic acid was synthesized according to the reported procedure.[21] IR820 (200 mg, 0.24 mmol) and TPE-Ph-boronic acid (0.16 g, 0.36 mmol) were dissolved in mixed solvents of toluene/ethanol/water (30 mL, v/v/v = 12:12:6). K_2CO_3 (0.17 g, 1.2 mmol) was added to the solution, and N_2 was bubbled through the solution for 30 min. After Pd $(PPh_3)_4$ (14 mg, 0.012 mmol) was added to the mixture, it was refluxed under N_2 atmosphere overnight. After removal of the solvent under reduced pressure, the obtained residue was purified by column chromatography using dichloromethane/methanol (7:3, v/v), resulting in a green solid (0.13 g, 45% yield). ^{1}H NMR (DMSO): δ 8.01(dd, J = 8.6, 3.6 Hz, 4H), 7.92 (d, J = 8.3 Hz, 4H), 7.72 (d, J = 8.6 Hz, 4H), 7.54-7.48 (m, 4H), 7.37 (d, J = 8.2 Hz, 2H), 7.30–7.13 (m, 17H), 7.06–7.03 (m, 2H), 6.31(d, J = 14.2 Hz, 2H), 4.25(s, 4H), 2.75(s, 4H), 2.49(d, J = 4.9 Hz, 4H, overlap with DMSO peaks), 2.00(d, J = 3.6 Hz, 2H). 1.80-1.74(m, 8H), 1.42(s, 12H) ^{13}C NMR (DMSO): δ 172.7, 160.9, 146.4, 143.8, 143.2, 141.5, 140.7, 140.4, 139.9, 138.3, 138.1, 133.1, 132.1, 131.7, 131.5, 131.3, 131.2, 130.8, 130.5, 130.4, 128.5, 128.4, 128.1, 127.9, 127.3, 127.2, 127.1, 126.7, 125.1, 122.4, 112.2, 100.4, 51.3, 50.4, 27.1, 26.8, 23.0. MALDI-TOF-MS calcd for $C_{72}H_{69}N_2O_6S_2$ $[M+2H]^+$: 1199.51, found: 1199.53.

Transient Absorption Spectroscopic Measurement: Femtosecond transient absorption (fs-TA) spectra were recorded using an ultrafast transient absorption spectrometer (HARPIA-TA, Light Conversion, Vilnius, Lithuania), consisting of a 6 kHz repetition rate femtosecond Yb:KGW amplifier laser (PHAROS, Light Conversion) and an optical parametric amplifier system (ORPHEUS, Light Conversion) in the National Research Facilities and Equipment Center (NanoBio-Energy Materials Center) at Ewha Womans University. Samples were prepared in 2 mm quartz cells and purged with 99.99% N_2 gas prior to excitation. The excitation pulse energy at 710 nm was adjusted ≈0.26 μJ pulse^{-1}.

Nanosecond transient absorption (ns-TA) data were acquired utilizing a home-built laser-flash photolysis system that consists of a 400–900 nm range continuous probe light from a halogen lamp, of which a detection wavelength was chosen with a monochromator (H10-UV, Horiba Jobin Yvon) interfaced with a PMT module (H10722-21 21P-01, Hamamatsu). Pump pulses were generated from a Nd:YAG based broadband nanosecond laser system (NT340, EKSPLA, 20-Hz repetition rate, 410–2600 nm), interfaced with an optical parametric oscillator (OPO). The excitation pulse energy was adjusted to ≈1.0 mJ pulse^{-1}. The change of probe signal intensity upon the photoexcitation was detected using a 500 MHz digital oscilloscope (TDS3052B, Tektronics). Samples were prepared in 1 cm quartz cells and purged with 99.99% N_2 gas before experiments.

Preparation and Characterizations of IR820@Exo, IR820-TPE@Exo, and IR820-TPE@B-Exo: Exosomes were prepared and extracted from HEK-293T human embryonic kidney cells using ExoQuick-TC (System Biosciences, Palo Alto, USA). IR820@Exo, IR820-TPE@Exo, and IR820-TPE@B-Exo were prepared by simple incubation of exosomes with IR820-TPE (or IR820). Detailed procedures are available in the Supporting Information. The concentrations of IR820 and IR820-TPE encapsulated in exosomes were determined based on their absorbance using UV–Vis spectroscopy. The following formula was used to quantify the encapsulation efficiencies of IR820 or IR820-TPE: (amount of IR820 or IR820-TPE loaded into exosomes)/(initial amount of added IR820 or IR820-TPE) × 100%. The size of the drug-loaded exosomes was measured by nanoparticle tracking analysis (NTA, Nanosight NS300) at 25 °C. The morphology of the drug-loaded exosomes was observed by TEM (Talos F200X, FEI, Hillsboro, OR, USA). The surface charges of various samples were measured using Zetasizer (Nano-ZS, Malvern). The expressions of typical exosome marker proteins were determined by western blotting, as previously reported.[22]

In Vitro PDT and SDT Evaluation: A conventional MTT assay was adopted to determine the cytotoxicity of IR820-TPE-based samples in MCF-7 cells, as was previously reported.[23] After MCF-7 cells were prepared in 96-well plates, 150 μL of FBS-free medium containing IR820, IR820-TPE, IR820@Exo, IR820-TPE@Exo, and IR820-TPE@B-Exo was added (5 μM of IR820 or IR820-TPE). The fresh culture medium was replaced after 4 h of treatment. The cells treated with various samples were subjected to either NIR light (808 nm, 500 mW, 2 min), US (1 MHz, 0.5 W cm^{-2}, 2 min), or a combination of both (2 min for each) to examine the NIR light- and US-triggered cytotoxicity of various samples. Cell viability was assessed 24 hours after the sample treatment, as previously described.[23]

In Vivo Antitumor Efficacy of IR820-TPE-Loaded Exosomes: All animal experiments at Incheon National University were approved by the institution animal care and use committee, and they were carried out by the protocol (INU-ANIM-2021-06). To prepare tumor-bearing animal models, 1×10^7 MCF-7 cells were subcutaneously injected into the back right side of Balb/nude mice (4-week-old male; Orient Bio, Gyeonggi-do, South Korea). When the tumor volume in the mice reached an average volume of 100 mm^3, the following formulations (100 μL) were injected into the tail vein: PBS, IR820-TPE, IR820@Exo, IR820-TPE@Exo, and IR820-TPE@B-Exo at the equivalent concentration of 100×10^{-6} M IR820 or IR820-TPE. After 4 h post-i.v. injection, the tumor site of mice was irradiated with NIR light (808 nm, 500 mW, 2 min), US (1 MHz, 0.5 W cm^{-2}, 2 min), or NIR light (2 min) + US (2 min). The tumor growth and body weight change were observed during 14 days. On the fourteenth day after sample treatment, the mice were euthanized using CO_2 gas. The tumors and major organs (liver, spleen, heart, lung, and kidney) of mice were collected and stained with hematoxylin and eosin (H&E).

Statistical Analysis: All the data were acquired in triplicate unless specified otherwise. Data were indicated as mean ± standard deviation (SD) values. Statistical significance between sample groups was determined by one-way ANOVA and represented as follows: $*p < 0.05$; $**p < 0.01$.

Supporting Information

Supporting Information is available from the Wiley Online Library or from the author.

© 2025 The Author(s). Advanced Healthcare Materials published by Wiley-VCH GmbH

21922659, 2025, 18, Downloaded from https://advanced.onlinelibrary.wiley.com/doi/10.1002/adhm.202500927 by Ewha Womans University Library, Wiley Online Library on [07/12/2025]. See the Terms and Conditions (https://onlinelibrary.wiley.com/terms-and-conditions) on Wiley Online Library for rules of use; OA articles are governed by the applicable Creative Commons License

Acknowledgements

V.-N.N., T.G.N.C., and H.J. contributed equally to this work. This work was supported by the National Research Foundation of Korea(NRF) grant funded by the Korea government(MSIT) (No. RS-2023-00217701 for J.Y., No. NRF-2022R1A2C1007207 for M.S.S., and No. NRF-RS-2023-00244402 for J.P). V.-N.N. acknowledges the support of the Basic Science Research Program through the National Research Foundation of Korea(NRF) funded by the Ministry of Education (2022R1I1A1A01055905). K.M. K.S. acknowledges the support of the Brain Pool program funded by the Ministry of Science and ICT through the National Research Foundation of Korea (2022H1D3A2A01096309). The ^{1}H NMR and ^{13}C NMR spectra as well as femtosecond transient absorption spectra were collected using a Bruker AM 300 and a HARPIA spectrometry system, respectively, at the National Research Facilities and Equipment Center (NanoBio·Energy Materials Center) at Ewha Womans University.

Conflict of Interest

The authors declare no conflict of interest.

Data Availability Statement

The data that support the findings of this study are available from the corresponding author upon reasonable request.

Keywords

cancer treatment, exosome, heptamethine cyanine, reactive oxygen species, sensitizer, sono-photodynamic therapy

Received: February 19, 2025
Revised: March 17, 2025
Published online: April 1, 2025

[1] a) X. Li, J. F. Lovell, J. Yoon, X. Chen, *Nat. Rev. Clin. Oncol.* **2020**, *17*, 657; b) C. W. Ng, J. Li, K. Pu, *Adv. Funct. Mater.* **2018**, *28*, 1804688; c) S. Son, J. H. Kim, X. Wang, C. Zhang, S. A. Yoon, J. Shin, A. Sharma, M. H. Lee, L. Cheng, J. Wu, J. S. Kim, *Chem. Soc. Rev.* **2020**, *49*, 3244; d) B. del Rosal, B. Jia, D. Jaque, *Adv. Funct. Mater.* **2018**, *28*, 1803733.

[2] a) H. Shigemitsu, K. Ohkubo, K. Sato, A. Bunno, T. Mori, Y. Osakada, M. Fujitsuka, T. Kida, *JACS Au* **2022**, *2*, 1472; b) K.-X. Teng, L.-Y. Niu, Q.-Z. Yang, *J. Am. Chem. Soc.* **2023**, *145*, 4081; c) M. Lan, S. Zhao, W. Liu, C.-S. Lee, W. Zhang, P. Wang, *Adv. Healthcare Mater.* **2019**, *8*, 1900132; d) V. N. Nguyen, Y. Yan, J. Zhao, J. Yoon, *Acc. Chem. Res.* **2021**, *54*, 207; e) V. N. Nguyen, S. Qi, S. Kim, N. Kwon, G. Kim, Y. Yim, S. Park, J. Yoon, *J. Am. Chem. Soc.* **2019**, *141*, 16243; f) S. Li, Q. Zou, Y. Li, C. Yuan, R. Xing, X. Yan, *J. Am. Chem. Soc.* **2018**, *140*, 10794; g) Y. Shen, A. J. Shuhendler, D. Ye, J. J. Xu, H. Y. Chen, *Chem. Soc. Rev.* **2016**, *45*, 6725.

[3] a) B. Gu, W. Wu, G. Xu, G. Feng, F. Yin, P. H. J. Chong, J. Qu, K. T. Yong, B. Liu, *Adv. Mater.* **2017**, 29; b) R. Chang, L. Zhao, R. Xing, J. Li, X. Yan, *Chem. Soc. Rev.* **2023**, *52*, 2688; c) R. Chang, Q. Zou, L. Zhao, Y. Liu, R. Xing, X. Yan, *Adv. Mater.* **2022**, *34*, 2200139.

[4] a) P. H. Zhao, Y. L. Wu, X. Y. Li, L. L. Feng, L. Zhang, B. Y. Zheng, M. R. Ke, J. D. Huang, *Angew. Chem., Int. Ed.* **2022**, *61*, 202113506; b) X. Wang, M. Wu, H. Li, J. Jiang, S. Zhou, W. Chen, C. Xie, X. Zhen, X. Jiang, *Adv. Sci.* **2022**, *9*, 2104125; c) X. Meng, S. Sun, C. Gong, J. Yang, Z. Yang, X. Zhang, H. Dong, *ACS Nano* **2022**, *17*, 1174; d) Y. Wang, Y. Xu, S. Dong, P. Wang, W. Chen, Z. Lu, D. Ye, B. Pan, D. Wu, C. D. Vecitis, G. Gao, *Nat. Commun.* **2021**, *12*, 3508; e) P. Huang, X. Qian, Y. Chen, L. Yu, H. Lin, L. Wang, Y. Zhu, J. Shi, *J. Am. Chem. Soc.* **2017**, *139*, 1275; f) B. Geng, J. Hu, Y. Li, S. Feng, D. Pan, L. Feng, L. Shen, *Nat. Commun.* **2022**, *13*, 5735.

[5] Y. Zheng, J. Ye, Z. Li, H. Chen, Y. Gao, *Acta Pharm. Sin. B.* **2021**, *11*, 2197.

[6] G. Zhao, S. Chen, J. Zheng, C. Li, X. Zhong, Y. Cao, Y. Zheng, J. Sun, S. Zhu, S. Chang, *J. Photochem. Photobiol. B: Biol.* **2023**, *238*, 112583.

[7] a) M. Liang, X. Mu, Y. Li, Y. Tan, X. Hao, Y. Tang, Z. Wang, W. Feng, Y. Lu, X. Zhou, *Adv. Funct. Mater.* **2023**, 2302112; b) H. Li, H. Kim, F. Xu, J. Han, Q. Yao, J. Wang, K. Pu, X. Peng, J. Yoon, *Chem. Soc. Rev.* **2022**, *51*, 1795; c) T. Liu, Y. Chen, H. Wang, M. Cui, J. Zhang, W. Zhang, P. Wang, *Adv. Healthcare Mater.* **2023**, *12*, 2202817.

[8] a) Y. Yang, J. Huang, M. Liu, Y. Qiu, Q. Chen, T. Zhao, Z. Xiao, Y. Yang, Y. Jiang, Q. Huang, K. Ai, *Adv. Sci.* **2023**, *10*, 2204365; b) B. Wu, Y. Yuan, J. Liu, H. Shang, J. Dong, X. Liang, D. Wang, Y. Chen, C. Wang, Y. Zhou, H. Jing, W. Cheng, *J. Nanobiotechnol.* **2021**, *19*, 177; c) Y. Li, Q. Zhou, Z. Deng, M. Pan, X. Liu, J. Wu, F. Yan, H. Zheng, *Sci. Rep.* **2016**, *6*, 25968.

[9] M. J. Mitchell, M. M. Billingsley, R. M. Haley, M. E. Wechsler, N. A. Peppas, R. Langer, *Nat. Rev. Drug Discovery* **2021**, *20*, 101.

[10] a) T. G. Nguyen Cao, Q. T. Hoang, J. H. Kang, S. J. Kang, V. Ravichandran, W. J. Rhee, M. Lee, Y. T. Ko, M. S. Shim, *Biomaterials* **2023**, *301*, 122242; b) Z. Chen, X. Yun, J. Tian, F. Li, Z. Zhang, J. Meng, N. Li, H. Bian, S. Duan, L. Zhang, *Adv. Healthcare Mater.* **2025**, *14*, 2570020; c) D. Zhu, Y. Duo, M. Suo, Y. Zhao, L. Xia, Z. Zheng, Y. Li, B. Z. Tang, *Angew. Chem., Int. Ed.* **2020**, *59*, 13836. d) I. K. Herrmann, M. J. A. Wood, G. Fuhrmann, *Nat. Nanotechnol.* **2021**, *16*, 748.

[11] W. X. Ren, J. Han, S. Uhm, Y. J. Jang, C. Kang, J.-H. Kim, J. S. Kim, *Chem. Commun.* **2015**, *51*, 10403.

[12] a) X. Yuan, Y. Tao, W. Xiao, K. Du, H. Hu, D. Xu, Q. Xu, *Drug Dev. Res.* **2022**, *83*, 1923; b) Z. Feng, X. Yu, M. Jiang, L. Zhu, Y. Zhang, W. Yang, W. Xi, G. Li, J. Qian, *Theranostics* **2019**, *9*, 5706; c) H. Hu, X. Liu, J. Hong, N. Ye, C. Xiao, J. Wang, Z. Li, D. Xu, *J. Colloid Interface Sci.* **2022**, *612*, 246.

[13] a) X. Zhao, H. Zhao, S. Wang, Z. Fan, Y. Ma, Y. Yin, W. Wang, R. Xi, M. Meng, *J. Am. Chem. Soc.* **2021**, *143*, 20828; b) X. Zhao, Q. Yao, S. Long, W. Chi, Y. Yang, D. Tan, X. Liu, H. Huang, W. Sun, J. Du, J. Fan, X. Peng, *J. Am. Chem. Soc.* **2021**, *143*, 12345.

[14] G. Bao, S. Wen, W. Wang, J. Zhou, S. Zha, Y. Liu, K. L. Wong, D. Jin, *Nano Lett.* **2021**, *21*, 9862.

[15] a) H. Huang, W. Xie, Q. Wan, L. Mao, D. Hu, H. Sun, X. Zhang, Y. Wei, *Adv. Sci.* **2022**, *9*, 2104101; b) J. Liu, S. Dong, S. Gai, Y. Dong, B. Liu, Z. Zhao, Y. Xie, L. Feng, P. Yang, J. Lin, *ACS Nano* **2023**, *17*, 20402.

[16] Q. T. Hoang, K. A. Huynh, T. G. Nguyen Cao, J. H. Kang, X. N. Dang, V. Ravichandran, H. C. Kang, M. Lee, J. E. Kim, Y. T. Ko, T. I. Lee, M. S. Shim, *Adv. Mater.* **2023**, *35*, 2300437.

[17] a) V.-N. Nguyen, J. Ha, C. W. Koh, B. Ryu, G. Kim, J. H. Park, C.-Y. Kim, S. Park, J. Yoon, *Chem. Mater.* **2021**, *33*, 7889; b) D. Rosenblum, N. Joshi, W. Tao, J. M. Karp, D. Peer, *Nat. Commun.* **2018**, *9*, 1410.

[18] a) X. Zhu, M. Badawi, S. Pomeroy, D. S. Sutaria, Z. Xie, A. Baek, J. Jiang, O. A. Elgamal, X. Mo, K. Perle, J. Chalmers, T. D. Schmittgen, M. A. Phelps, *J. Extracell. Vesicles* **2017**, *6*, 1324730; b) J. Li, X. Chen, J. Yi, Y. Liu, D. Li, J. Wang, D. Hou, X. Jiang, J. Zhang, J. Wang, K. Zen, F. Yang, C. Y. Zhang, Y. Zhang, *PLoS One* **2016**, *11*, 0163043.

[19] I. Prada, J. Meldolesi, *Int. J. Mol. Sci.* **2016**, *17*, 1296.

[20] N. Bie, T. Yong, Z. Wei, L. Gan, X. Yang, *Adv. Drug Delivery Rev.* **2022**, *188*, 114450.

[21] H. Li, Z. Chi, B. Xu, X. Zhang, X. Li, S. Liu, Y. Zhang, J. Xu, *J. Mater. Chem.* **2011**, *21*, 3760.

[22] H. C. Yang, W. J. Rhee, *J. Clin. Med.* **2021**, *10*, 319.

[23] T. G. Nguyen Cao, Q. T. Hoang, E. J. Hong, S. J. Kang, J. H. Kang, V. Ravichandran, H. C. Kang, Y. T. Ko, W. J. Rhee, M. S. Shim, *J. Controlled Release* **2023**, *354*, 651.

© 2025 The Author(s). Advanced Healthcare Materials published by Wiley-VCH GmbH

21922659, 2025, 18, Downloaded from https://advanced.onlinelibrary.wiley.com/doi/10.1002/adhm.202500927 by Ewha Womans University Library, Wiley Online Library on [07/12/2025]. See the Terms and Conditions (https://onlinelibrary.wiley.com/terms-and-conditions) on Wiley Online Library for rules of use; OA articles are governed by the applicable Creative Commons License